Electronic Supplementary Information (ESI) for

Push-pull type *meso*-ester substituted BODIPY near-infrared dyes as contrast agents for photo-acoustic imaging

Table of Contents

1. Experimental Section

1.1 General

All reagents were purchased from commercial suppliers and used as received without further purification. Anhydrous dichloromethane (DCM) was distilled from CaH_2, anhydrous THF and toluene were distilled from sodium. The ^1H NMR and ^{13}C NMR spectra were recorded in solution of $CDCl_3$ on Bruker DPX 300 or DRX 500 NMR spectrometers with tetramethylsilane (TMS) as the internal standard. The following abbreviations were used to explain the multiplicities: s = singlet, d = doublet, t = triplet, m = multiplet. MALDI-TOF mass spectra were measured on a Bruker Autoflex MALDI-TOF instrument using 1,8,9- trihydroxyanthracene as a matrix. HR-ESI mass spectra were recorded on Thermo-Finnigan LCQ mass spectrometer. UV-Vis-NIR absorption spectra were recorded on a Shimadzu UV-1700 spectrometer. The solvents used for UV-Vis and fluorescence measurements are of HPLC grade. The electrochemical measurements were carried out in anhydrous DCM with 0.1 M tetrabutylammonium hexafluorophosphate (Bu_4NPF_6) as the supporting electrolyte at a scan rate of 0.05 V/s at room temperature under the protection of nitrogen.

1.2 Synthetic procedures and characterization data

The synthesis of aldehyde intermediates **8** and **9** is show in Scheme S1. Compound **5** was synthesized according to our previous report.[1]

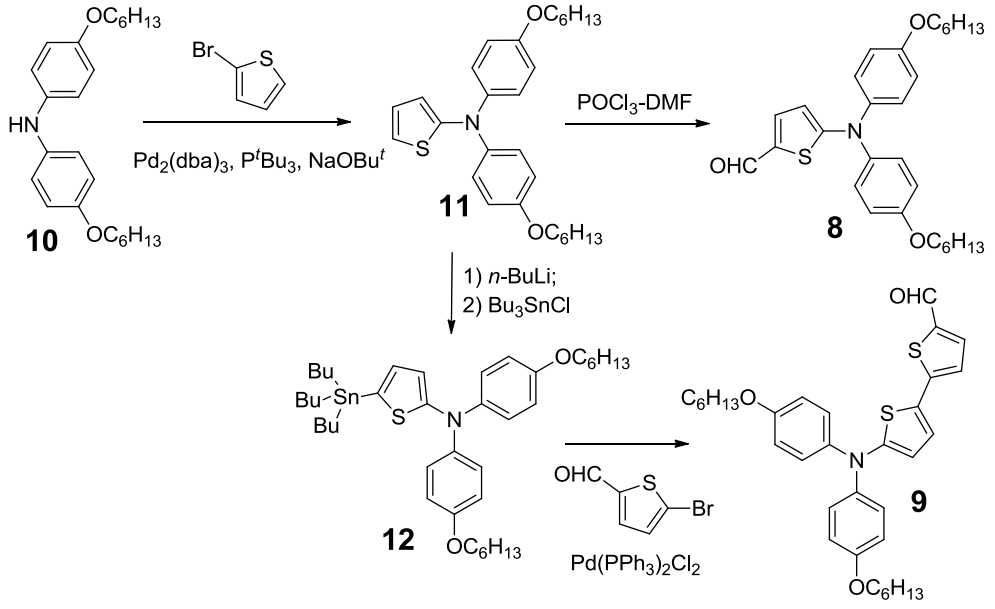

Scheme S1. Synthetic route of aldehydes **8** and **9**.

Compound 8: To a 100 mL round-bottomed flask, anhydrous deoxygenated toluene (20 mL), $Pd_2(dba)_3$ (0.091 g, 0.10 mmol), and P*t*Bu_3 (0.25 mmol, 10% weight solution in hexanes, Strem) were added under nitrogen. The solution was stirred at room temperature under nitrogen for 20 min. Compound **10** (2.84 g, 7.70 mmol), 2-bromothiophene (3.2 g, 20 mmol), and sodium *tert*-butoxide (3.0 g, 31mmol) were added. The reaction mixture was heated to reflux under nitrogen. After 5 h of heating, the reaction appeared complete as followed by TLC (silica gel, 5% ethyl acetate in hexanes), and the solvent was removed by rotary evaporation. The crude product was re-dissolved in 5% ethyl acetate in hexanes and was passed through a plug of silica gel, eluting with the same solvent. The solvent was removed and the crude product **11** was used directly for next step.

Phosphorus oxychloride (0.98 g, 6.43 mmol) was added dropwise to a stirred mixture of **11** (2.80 g, 5.84 mmol) and anhydrous *N*,*N*-dimethylformamide (20 mL) at 0 °C under nitrogen. The reaction mixture was stirred for 4 h at 0 °C after which the reaction was brought to room temperature for 1 h. The reaction mixture was poured into aqueous sodium carbonate, and a yellow-orange precipitate formed. The aqueous layer was extracted with ethyl acetate, and the organic layer was subsequently washed with aqueous sodium carbonate and water, dried over magnesium sulfate. The solvent was removed and the residue was purified by column chromatography (silica gel, Hex:EA = 6:1) to give compound **8** as a yellow oil (2.37 g, 80 %). ^{1}H NMR (400 MHz, $CDCl_3$): δ 9.44 (s, 1H), 7.34 – 7.27 (m, 1H), 7.13 (d, *J* = 7.1 Hz, 4H), 6.79 (d, *J* = 7.1 Hz, 4H), 6.08 (d, *J* = 2.7 Hz, 1H), 3.86 (t, *J* = 5.8 Hz, 4H), 1.73 – 1.66 (m, 4H), 1.41 – 1.34 (m, 4H), 1.26 (s, 8H), 0.83 (s, 6H). ^{13}C NMR (101 MHz, $CDCl_3$): δ 180.85, 166.31, 157.54, 138.92, 138.60, 128.51, 127.07, 115.48, 108.96, 68.24, 31.50, 29.13, 25.65, 22.54, 13.97. HR-MS (MALDI-TOF) m/z = 479.2451 ($[M]^+$), calcd for $C_{29}H_{37}NO_3S$: 479.2494.

Compound 9: To a solution of compound **11** (2.26 g, 5 mmol) in dry THF (20 mL) at -78 °C under nitrogen was added *n*-butyl lithium (3.75 mL, 1.6 M in hexanes, 6 mmol). The solution was stirred for 5 min. then warmed to ambient temperature. The solution was then cooled with an ice/water bath, tri-*n*-butylchlorostannane (35 mL, 130 mmol) was added and the reaction was stirred overnight. The mixture was then added to brine. The aqueous layer was extracted with methylene chloride. The combined organic layers were dried with magnesium sulfate, and the solvent was removed in vacuo to give the product **12** contaminated with tri-n-butylchlorostannane residue. The product was used without further purification.

To a degassed solution of 5-bromo-2-thiophenecarboxaldehyde (0.42 g, 2.2 mmol) and compound **12** (1.36 g, 2.2 mmol) in DMF (10 mL) was added bis(triphenylphosphine)palladium(II) chloride (56 mg, 0.08 mmol). The mixture was heated to 80 °C for 10 min, then cooled to 40 °C, and stirred under nitrogen for 5 h. The reaction mixture was poured into aqueous sodium carbonate, and a yellow-orange

precipitate formed. The aqueous layer was extracted with ethyl acetate, and the organic layer was subsequently washed with aqueous sodium carbonate and water. The organic layer was dried with magnesium sulfate, filtered, and concentrated by rotary evaporation. Chromatography on a column of silica gel (Hex:EA = 6:1) gave compound **9** as a red-orange oil (1.76 g, 70%). ^{1}H NMR (400 MHz, $CDCl_3$): δ 9.68 (s, 1H), 7.48 (d, *J* = 4.0 Hz, 1H), 7.06 (d, *J* = 8.9 Hz, 4H), 6.99 (d, *J* = 4.1 Hz, 1H), 6.87 (d, *J* = 3.9 Hz, 1H), 6.76 (d, *J* = 8.9 Hz, 4H), 6.18 (d, *J* = 4.0 Hz, 1H), 3.86 (t, *J* = 6.5 Hz, 4H), 1.73 – 1.65 (m, 4H), 1.41 – 1.34 (m, 4H), 1.30 – 1.23 (m, 8H), 0.83 (s, 6H). ^{13}C NMR (100 MHz, $CDCl_3$): δ 182.09, 157.16, 156.50, 148.86, 140.26, 139.71, 137.84, 126.16, 125.87, 123.85, 121.86, 115.38, 113.41, 68.38, 31.67, 29.35, 25.83, 22.69, 14.12. HR-MS (MALDI-TOF) m/z = 561.2361 ($[M]^+$),calcd for $C_{33}H_{39}NO_3S_2$: 561.2372.

General procedure for the Knoevenagel condensation: In a round bottom flask equipped with a Dean stark apparatus, the corresponding aldehyde (2.2 eq), piperidine (2 mL) and AcOH (2 mL) were added to a solution of BODIPY **5** (1 mmol) in toluene (20 mL). The solution was heated at reflux for 12 hours. After cooling to room temperature, the mixture was washed three times with water. The organic phase was dried over $MgSO_4$ and the solvent was evaporated under reduced pressure. The residue was purified by silica gel column chromatography to afford the desired compounds **1**, **2**, **3** and **4**.

Compound 1: Yield 42%. ^{1}H NMR (400 MHz, $CDCl_3$): δ 7.42 (m, 6H), 7.14 (d, *J* = 16.1 Hz, 2H), 6.74 – 6.49 (m, 6H), 3.94 (s, 3H), 3.04 (s, 12H), 2.14 (s, 6H). ^{13}C NMR (101 MHz, $CDCl_3$): δ 165.94, 153.78, 150.59, 137.94, 137.01, 130.38, 129.16, 127.52, 124.87, 117.00, 114.78, 112.00, 52.33, 39.95, 12.61. HR-MS (ESI): *m/z* = 569.2888 ($[M+H]^+$), calcd for $C_{33}H_{35}BF_2N_4O_2$: 569.2900.

Compound 2: Yield 39%. ^{1}H NMR (400 MHz, $CDCl_3$): δ 7.31 (m, 6H), 7.00 (m, 10H), 6.75 (m, 12H), 6.54 (s, 2H), 3.85 (m, 11H), 2.05 (m, 6H), 1.71 (m, 8H), 1.45 – 1.26 (m, 24H), 0.86 (m, 12H) ppm. ^{13}C NMR(100 MHz, $CDCl_3$): δ 165.87, 155.77, 153.69, 149.45, 139.59, 138.35, 136.57, 130.63, 128.63, 128.15, 126.86, 123.48, 119.30, 117.25, 116.02, 115.17 , 52.44, 31.66, 29.34, 25.82, 22.74, 14.09, 12.57 ppm. HR-MS (ESI): *m/z* = 1217.7077 ($[M+H]^+$), calcd for $C_{77}H_{91}BF_2N_4O_6$: 1217.7084.

Compound 3: Yield 40%. ^{1}H NMR (400 MHz, $CDCl_3$): δ 7.68 – 5.38 (m, 26H), 3.85 (m, 11H), 2.03 (m, 6H), 1.68 (m, 8H), 1.45 – 1.15 (m, 24H), 0.84 (m, 12H) ppm. ^{13}C NMR (100 MHz, $CDCl_3$): δ 165.92, 157.29, 156.13, 152.68, 139.76, 137.44, 130.82, 129.79, 129.37, 125.91, 125.85, 125.60, 123.48, 117.28, 115.06, 113.62, 67.93, 52.21, 31.66, 29.34, 25.83, 22.79, 14.12, 12.53 ppm. HR-MS (MALDI-TOF): *m/z* = 1228.6114 ($[M]^+$), calcd for $C_{73}H_{87}BF_2N_4O_6S_2$: 1228.6128.

Compound 4: Yield 37%. ^{1}H NMR (400 MHz, $CDCl_3$): δ 7.19 (m, 4H), 7.00 (m, 10H), 6.90 (d, *J* = 4.0 Hz, 2H), 6.77 (d, *J* = 3.8 Hz, 2H), 6.71 (d, *J* = 8.8 Hz, 8H), 6.53 (s, 2H), 6.23 (d, *J* = 4.0 Hz, 2H), 3.85 (m, 11H), 2.07 (m, 6H), 1.69 (m, 8H), 1.44 – 1.26 (m,

24H), 0.86 (m, 12H) ppm. ^{13}C NMR (100 MHz, $CDCl_3$): δ 155.71, 154.32, 152.78, 140.94, 140.36, 139.54, 138.44, 131.24, 130.05, 129.83, 129.12, 126.42, 125.03, 123.86, 122.61, 117.68, 117.24, 115.01, 68.00, 52.44, 31.68, 29.36, 25.84, 22.79, 14.12, 12.59 ppm. HR-MS (ESI): *m/z* = 1393.5945 ($[M+H]^+$), calcd for $C_{81}H_{91}BF_2N_4O_6S_4$: 1393.5968.

2. TD-DFT calculations

Time-dependent DFT (TD-DFT) calculations have been performed at the B3LYP/6-31G* level of theory,[2] as implemented in the *Gaussian 09* program package.[3] The geometries of **1**, **2, 3** and **4** were fully optimized in gas phase using the default convergence criteria without any constraints and confirmed by frequency calculations. The hexoxy groups are replaced by method groups during the calculations. UV-vis-NIR absorption spectra were generated assuming an average UV-vis width of 3000 cm^{-1} at half-height using the GaussSum program.

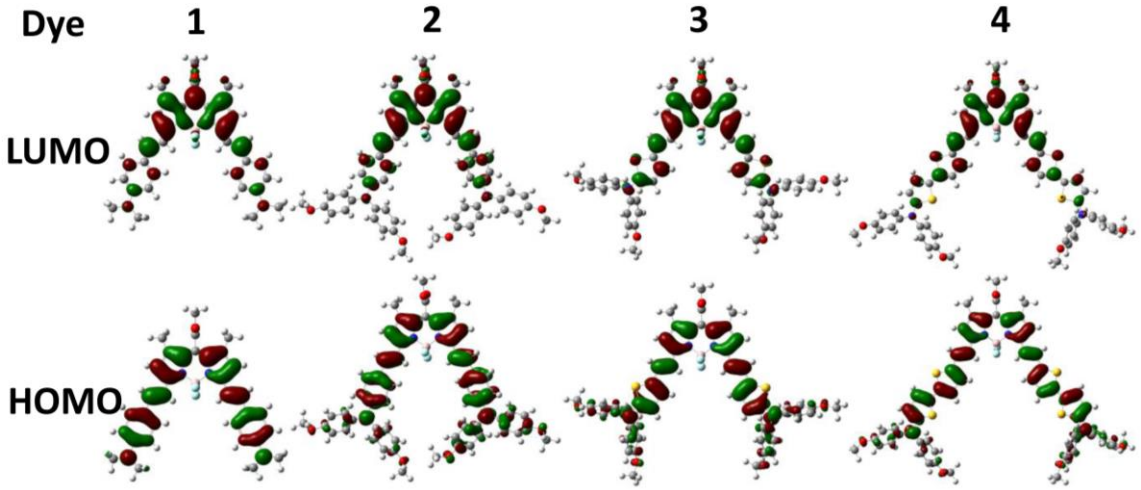

Fig. S1 Calculated frontier molecular orbital profiles of compounds **1**, **2**, **3** and **4**.

Wavelength (nm)	Osc. Strength	Major contributions
639.12	1.0014	HOMO->LUMO (101%)
500.25	0.3092	H-1->LUMO (91%)
413.16	0.0753	H-2->LUMO (87%)
365.60	1.1811	HOMO->L+1 (85%)

Table S1 Selected TD-DFT (B3LYP/6-31G*) calculated energies, oscillator strength and compositions of major electronic transitions of **1**.

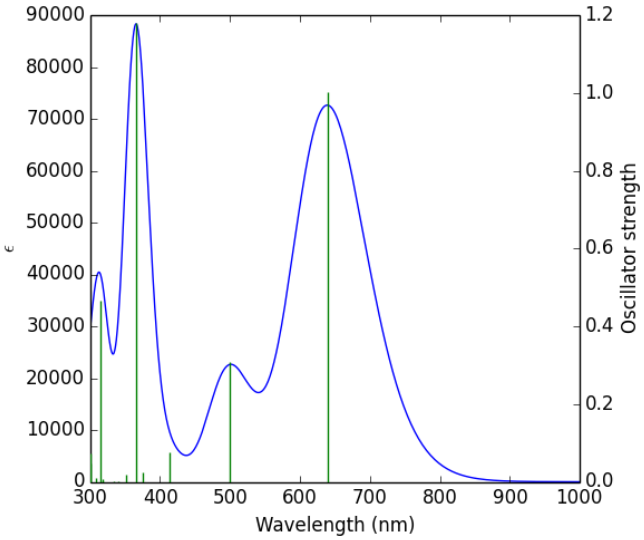

Fig. S2 Calculated absorption spectrum of **1**.

Wavelength (nm)	**Osc. Strength**	**Major contributions**
717.16	0.7556	HOMO->LUMO (98%)
590.42	0.422	H-1->LUMO (97%)
482.50	0.2486	H-2->LUMO (93%)
405.26	0.3862	H-3->LUMO (35%), HOMO->L+1 (62%)

Table S2 Selected TD-DFT (B3LYP/6-31G*) calculated energies, oscillator strength and compositions of major electronic transitions of **2**.

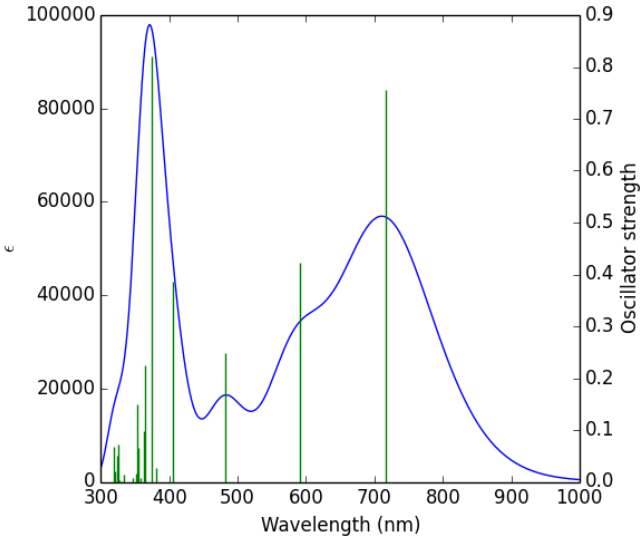

Fig. S3 Calculated absorption spectrum of **2**.

Wavelength (nm)	Osc. Strength	Major contribs
752.83	1.1883	HOMO->LUMO (99%)
609.19	0.3117	H-1->LUMO (94%)
489.24	0.1892	H-2->LUMO (91%)
442.31	0.6746	H-3->LUMO (15%), HOMO->L+1 (79%)

Table S3 Selected TD-DFT (B3LYP/6-31G*) calculated energies, oscillator strength and compositions of major electronic transitions of **3**.

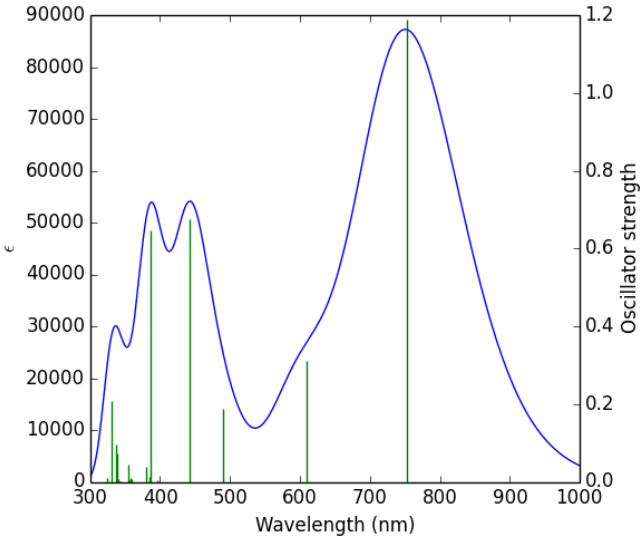

Fig. S4 Calculated absorption spectrum of **3**.

Wavelength (nm)	**Osc. Strength**	**Major contribs**
823.86	1.2228	HOMO->LUMO (98%)
695.68	0.367	H-1->LUMO (96%)
566.96	0.3457	H-2->LUMO (91%)
503.40	0.5875	H-3->LUMO (25%), HOMO->L+1 (71%)

Table S4 Selected TD-DFT (B3LYP/6-31G*) calculated energies, oscillator strength and compositions of major electronic transitions of **4.**

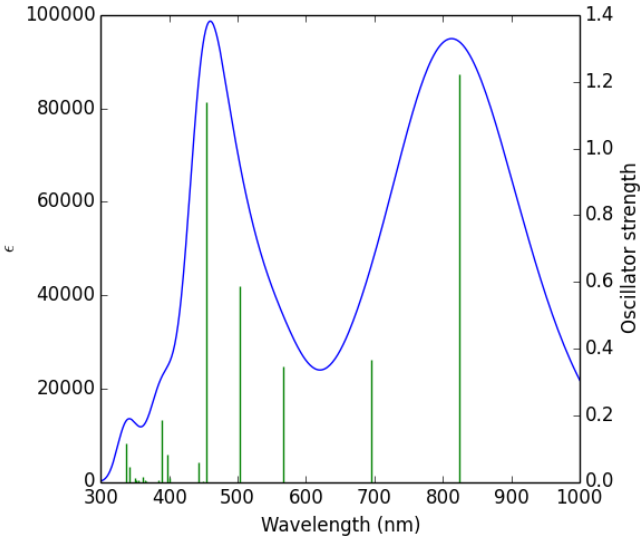

Fig. S5 Calculated absorption spectrum of **4.**

3. Electrochemical properties and photo-stability tests

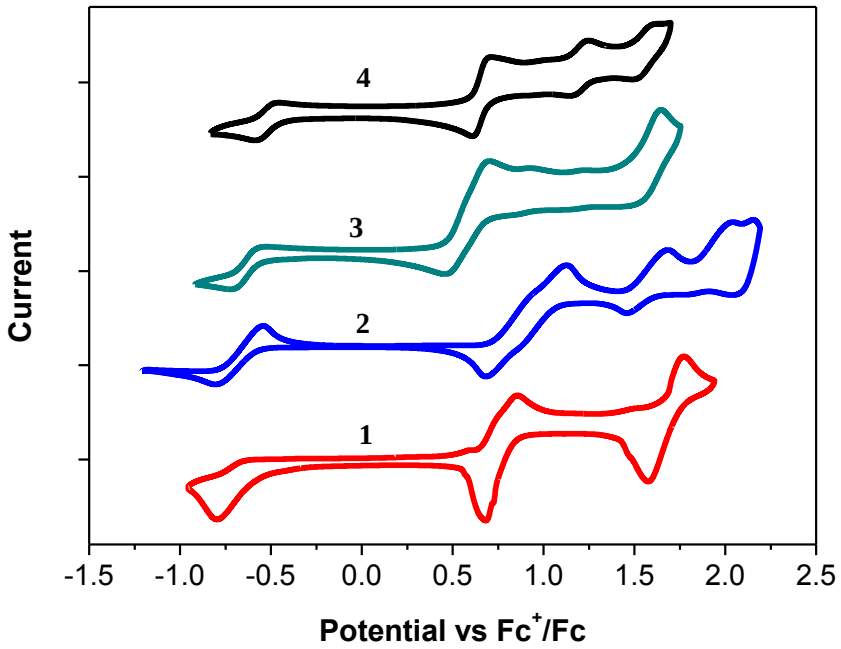

Fig. S6 Cyclic voltammograms of compounds **1**, **2**, **3** and **4** in dry DCM with 0.1 M Bu_4NPF_6 as a supporting electrolyte, AgCl/Ag as a reference electrode, Au disk as a working electrode, Pt wire as a counter electrode, and a scan rate of 50 mV· s^{-1}, Fc^+/Fc was used as external reference.

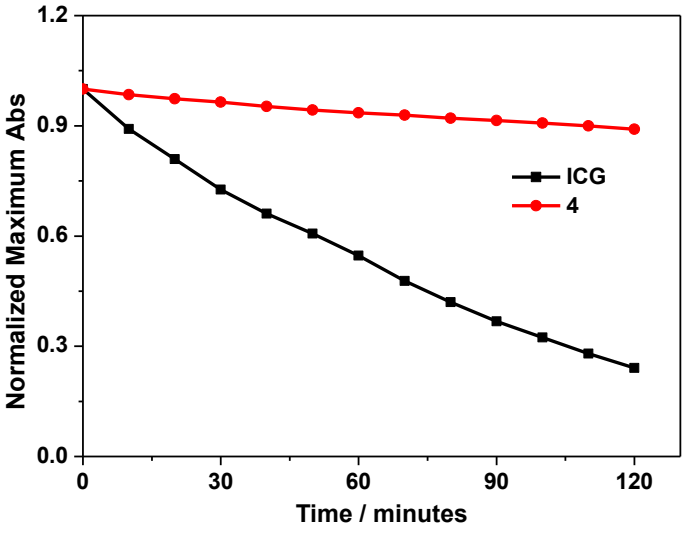

Fig. S7 Decay of compound **4** and ICG dye in toluene under irradiation of 100W white light bulb. The optical density at the absorption maximum was plotted with the irradiation time.

4. Fabrication and characterization of dye 4 loaded BSA NPs

Fabrication of dye 4 loaded BSA NPs: The NPs were prepared with feeding ratios ranging from 1.0 wt%, defined as the ratio of the weight of the dye **4** to that of the BSA in the feed mixture. In brief, 13 mg of BSA were dissolved in 5 mL of Milli-Q water. Subsequently, 2 mL of THF containing a predetermined amount of **4** were added dropwise into the aqueous solution of BSA under sonication at room temperature, using a microtip probe sonicator with an 18 W output (XL2000, Misonix Incorp., USA), leading to the formation of dye **4** loaded BSA NPs (the mixture would be somehow heated due to sonication). Until the mixture cooled down to room temperature, a small amount (100 μL) of glutaraldehyde solution (2.5%) was then added to cross-link the NPs at RT for 4 h. The THF was removed by rotary evaporation under vacuum. The cross-linked **4** loaded BSA-NP suspension was filtered through a 0.45 μm microfilter and was then washed with Milli-Q water. The amounts of the dyes successfully encapsulated into the BSA NPs were determined from the absorption spectra with reference to a calibration curve established from dimethyl sulfoxide (DMSO) solutions of **4**. The EE is defined as the ratio of the amount of the dye **4** loaded in the NPs to the total amount of the **4** in the feed mixture.

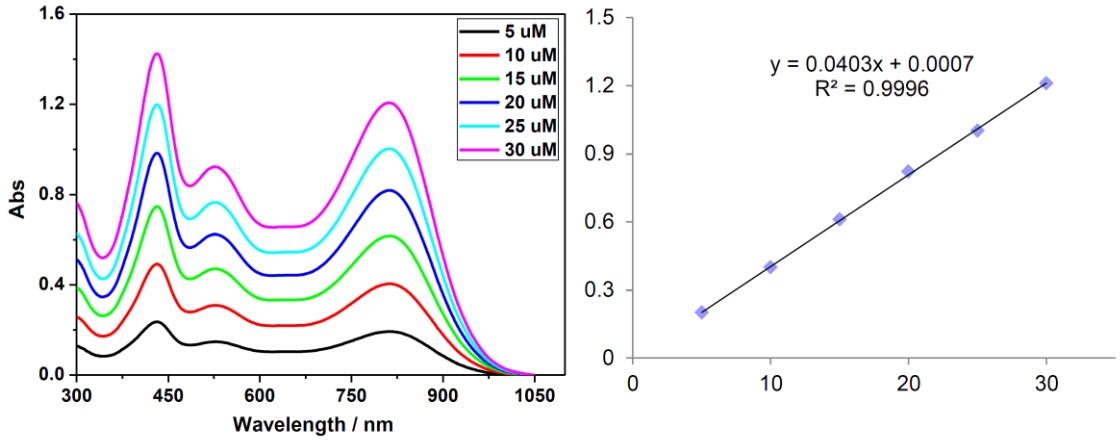

Fig. S8 Concentration dependent absorption specta of **4** in DMSO solution (a) and the calibration curve (b).

5. Methods and results of photoacoustic imaging (PAI)

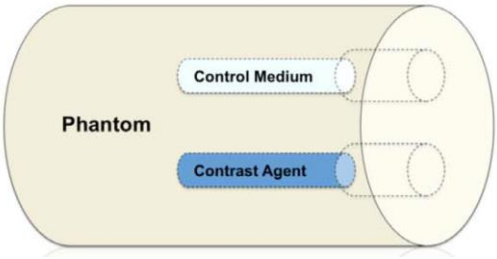

Fig. S9. Schematic tissue-mimicking phantom.

MSOT experimental parameters and protocol. All phantom and *in vivo* mouse imaging experiments were performed using a real-time multispectral optacoustic tomographic (MSOT) imaging system; inVision 64 (iThera Medical GmbH, Neuherberg, Germany).The phantom is made of polyurethane, cylindrical in shape with a diameter of 2 cm, which is specially designed to mimic the shape, size and optical properties of the mouse (iThera Medical GmbH, Neuherberg, Germany). In addition, it has 2 inner cylindrical channels, each with a diameter of 3 mm, one for holding the control medium and the other for holding the dissolved contrast agent in the same medium, as shown in Fig. S3. Optical excitation was provided by an optical parametric oscillator (OPO) with a tunable NIR wavelength range from 680 to 980 nm, which is in turn pumped by a Q-switched Nd:YAG laser with a pulse duration of 10 ns and repetition rate of 10 Hz. Light was delivered by a fiber bundle divided into 10 output arms to illuminate the sample from multiple angles around the imaging plane. PA signals were acquired using a 64-element concave transducer array spanning a circular arc of 270^{o}. This transducer array has a central frequency of 5 MHz, which provided a transverse spatial resolution in the range of 150–200 mm. One transverse image slice was acquired from each laser pulse, resulting in a frame-rate of 10 Hz. During image acquisition, the sample is translated through the transducer array along its axis across the volume ROI, in order to capture the corresponding transverse image slices. For *in vivo* imaging, clear ultrasound gel was applied on the mouse skin surface and measurements were recorded in temperature-controlled water for good acoustic coupling. An animal holder with a thin polyethylene membrane was used to prevent direct contact between the mouse and the water. The animal stage allows in-plane object translation over 150 mm with 0.1 mm

grid size for data acquisition. For generating photoacoustic signals the MSOT system consists of a 680 - 980 nm nanosecond pulsed laser with an average power density of 0.5 mJ cm^{-2} and is able to achieve a tomographic view of 172° with a curved detector containing 64-element array transducer. Signals obtained are then processed to reconstruct the anatomical and functional (multispectral) tomographic images using the integrated *ViewMSOT* software. Prior to placing the animal in the scanning chamber the animal is anesthetized in an isoflurane chamber. During the scan period the animal is placed in a belly down position and anesthetized by continuously maintaining the isoflurane at 1.5 – 2 % at an oxygen flow rate of 0.8 – 1.5 mL/min. The multispectral tomographic images were obtained by averaging 5 sample sets per wavelength.

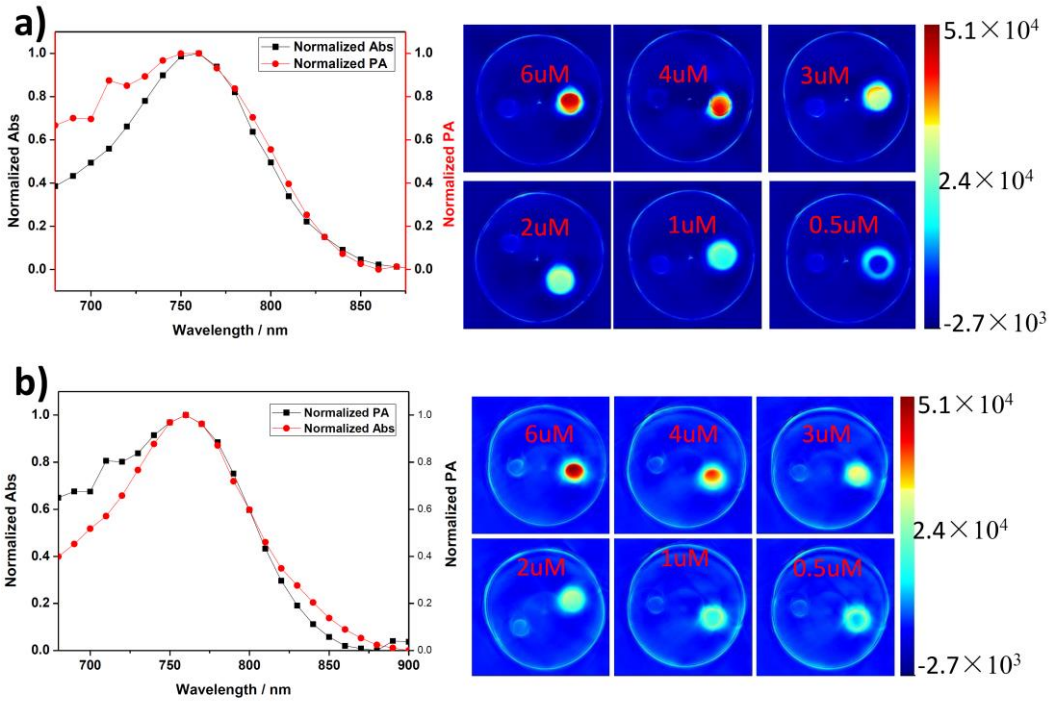

Fig. S10 Normalized Abs and PA spectrum of **1** [a) left curve] and **2** [b) left curve], concentration dependent PA images of **1** [a) right image] and **2** [b) right image] in DMSO solution from phantom test.

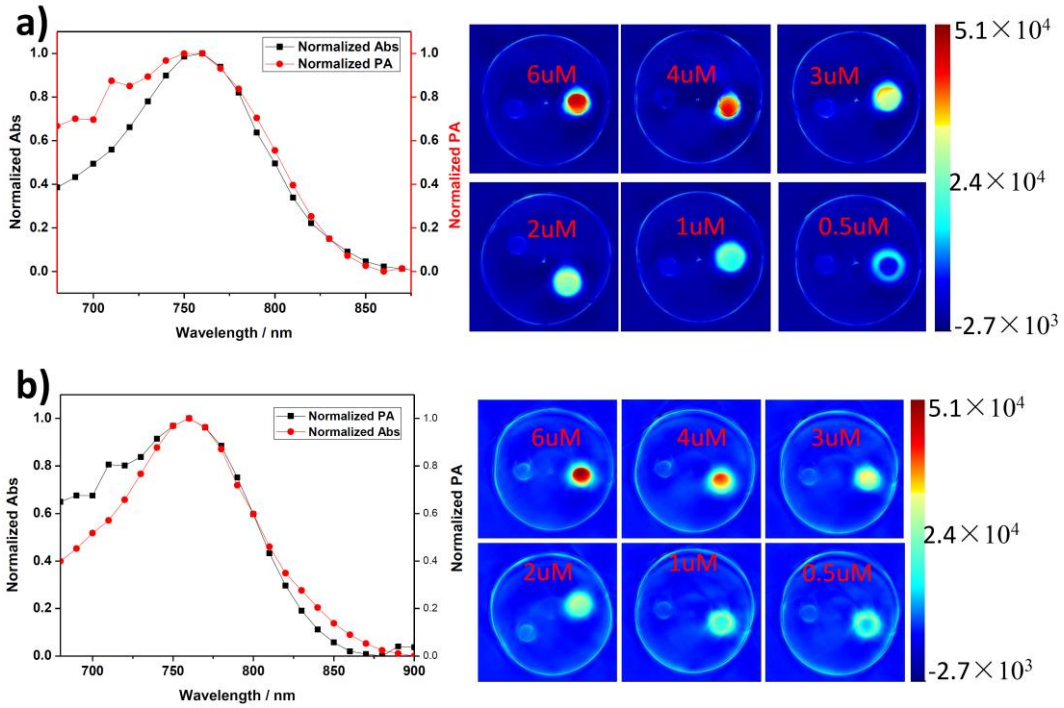

Fig. S11 Normalized Abs and PA spectrum of **3** [a) left curve] and **4** [b) left curve], concentration dependent PA images of **3** [a) right image after 2 μM the signal was saturated] and **4** [b) right image] in DMSO solution from phantom test.

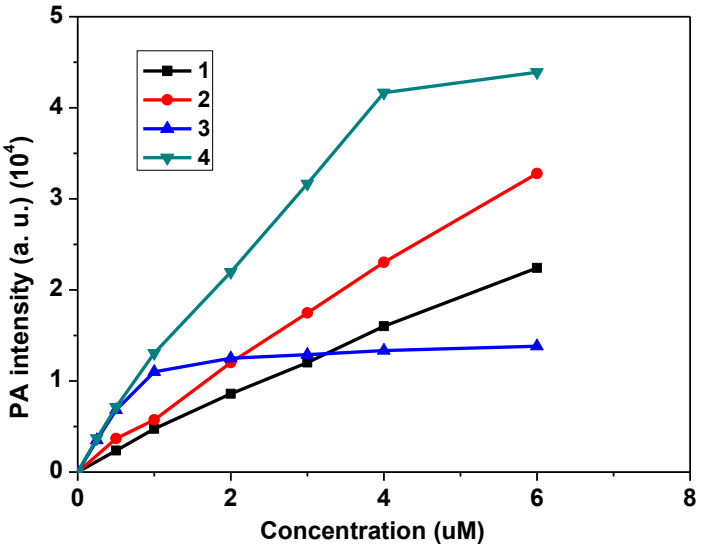

Fig. S12 Concentration dependent PA intensity curve of **1** (black), **2** (red), **3** (blue), **4** (cyan) in DMSO solution from phantom test.

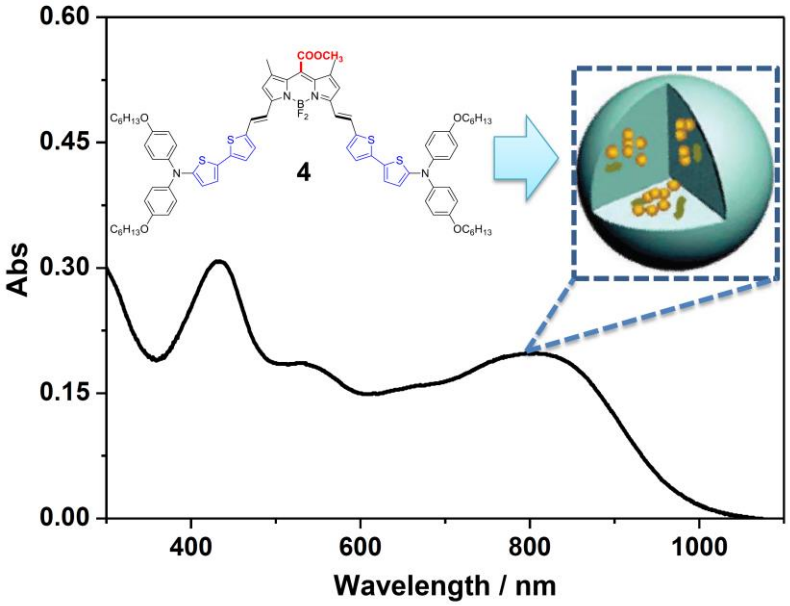

Fig. S13 Absorption spectrum of **4** loaded BSA NPs in aqueous solution that was used for photoacoustic phantom test. According to the calibration curve of **4**, the concentration of the **4** loaded BSA NPs was estimated as 6.738 μg·mL^{-1}. For the concentration dependent photoacoustic test, the other concentration of the NPs was diluted from this solution, by 2, 4, 8, 16 times respectively.

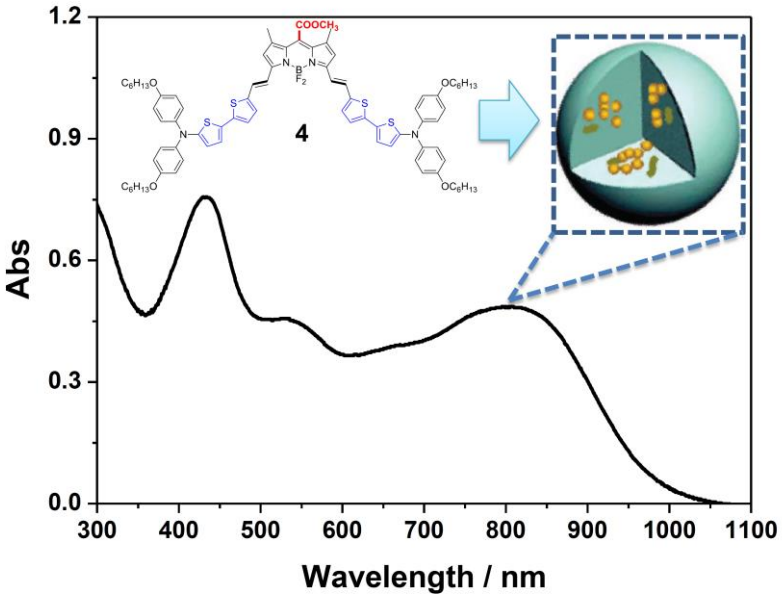

Fig. S14 Absorption spectrum of **4** loaded BSA NPs solution injected to Hep-G2-tumor mice (diluted by 10 times).

For the dye **4** loaded BSA NPs solution that would be injected to the Hep-G2-tumor mice, it was firstly diluted by 10 times before measuring the absorption spectrum (since

the solution was too concentrated, and the absorption would be saturated), the absorption spectrum was then measured, as shown in Fig. S8, the concentration of the **4** loaded BSA NPs injected to Hep-G2-tumor mice was estimated to be 165.6 μg/mL referring to the calibration curve.

6. Cell culture and preparation of Hep-G2-tumor mouse model

Hep-G2 liver cancer cells were cultured in Dulbecco's Modified Eagle's Medium (DMEM) containing 10% fetal bovine serum (FBS) and 1% penicillin streptomycin at 37°C in an incubator containing 5% CO2. When 80-90% confluent, cells were used for subcutaneous innoculation. Xenograft models were established by subcutaneous injection of 5×10^6 cells on the right flank of a Balb/C nude mouse. The mouse was continuously monitored for the tumor growth and was used for further experiments when the tumor volume reached a size of 1000 mm^3.

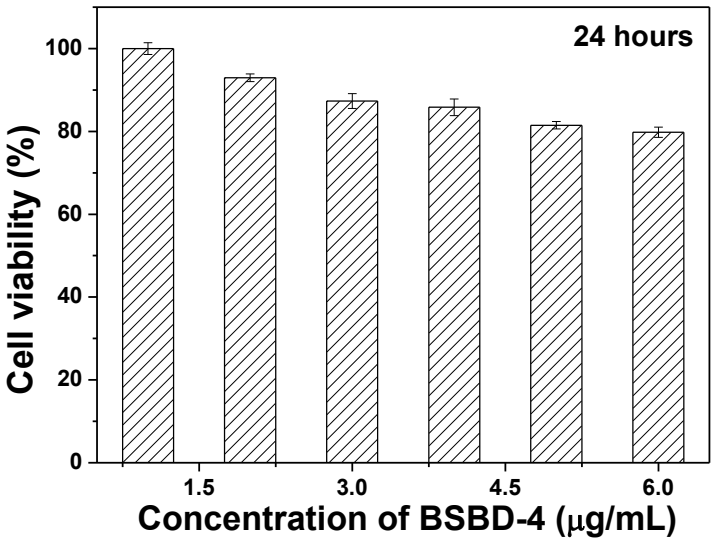

Fig. S15 Cell viability values (%) estimated by MTT proliferation tests versus incubation concentrations of dye **4** loaded BSA NPs. HeLa cells were cultured in the presence of dye **4** loaded BSA NPs at 37 ^oC for 24 h.

7. Appendix: ^{1}H, ^{13}C NMR, HR mass spectra of new compounds

Compound **8**: ^{1}H NMR ($CDCl_3$, 400 MHz):

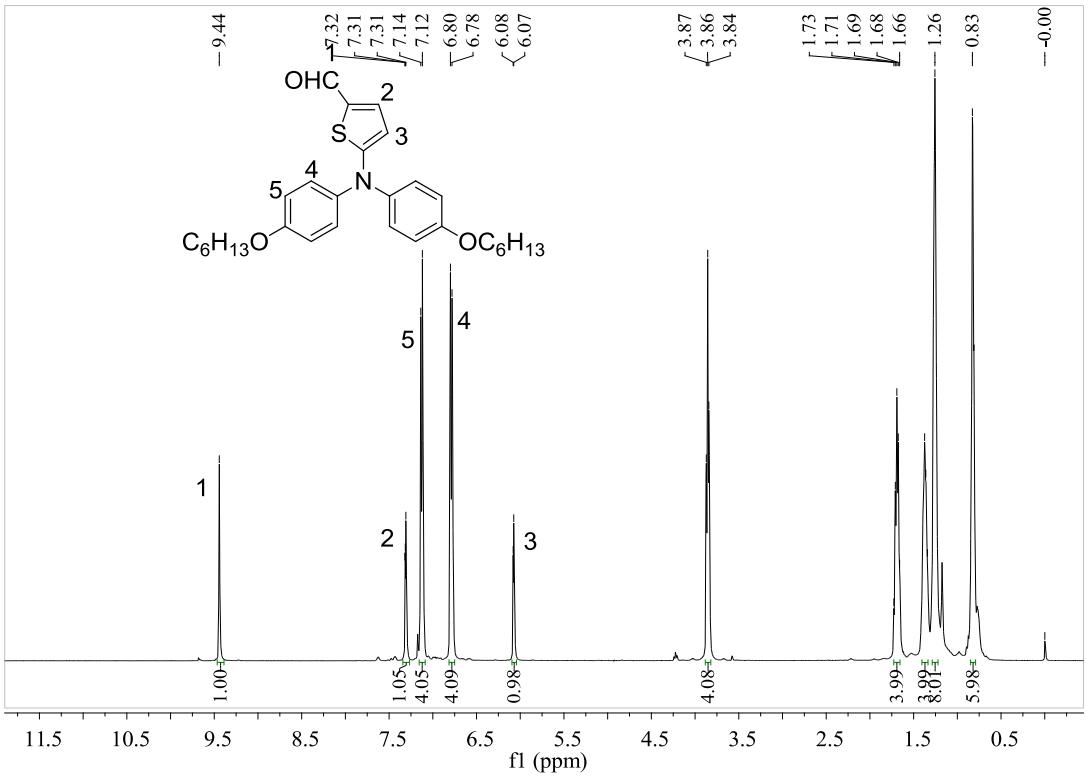

Compound **8**: ^{13}C NMR ($CDCl_3$, 100 MHz):

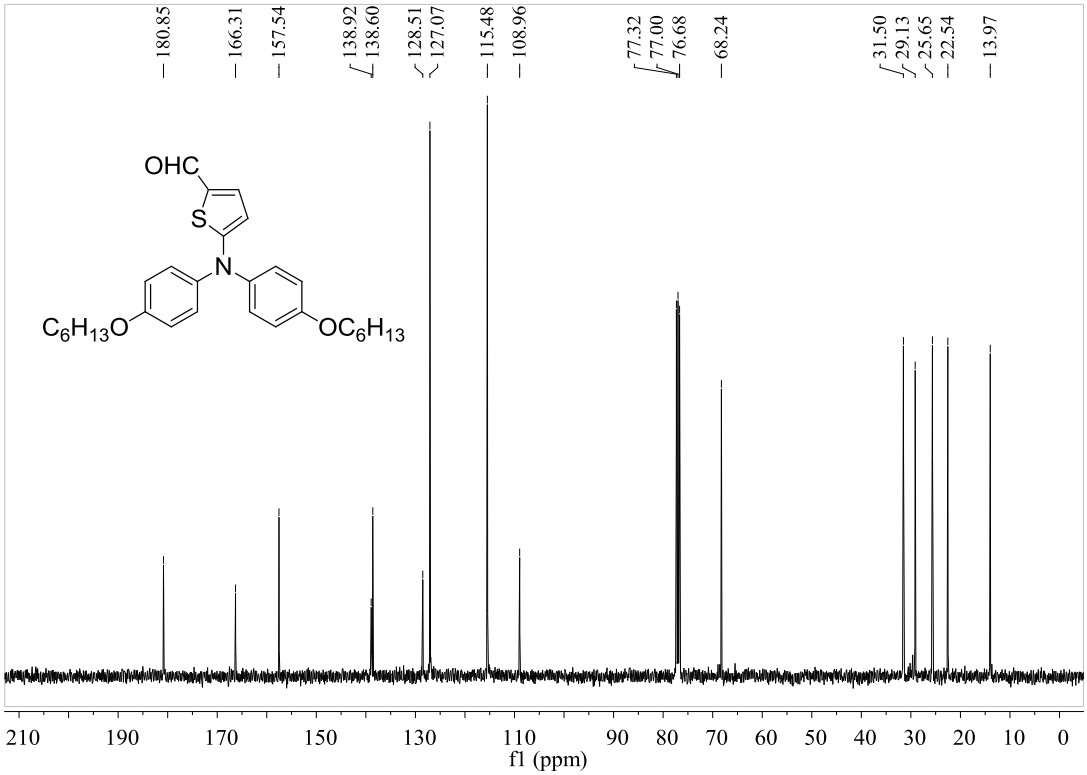

Compound **9**: ^{1}H NMR ($CDCl_3$, 400 MHz):

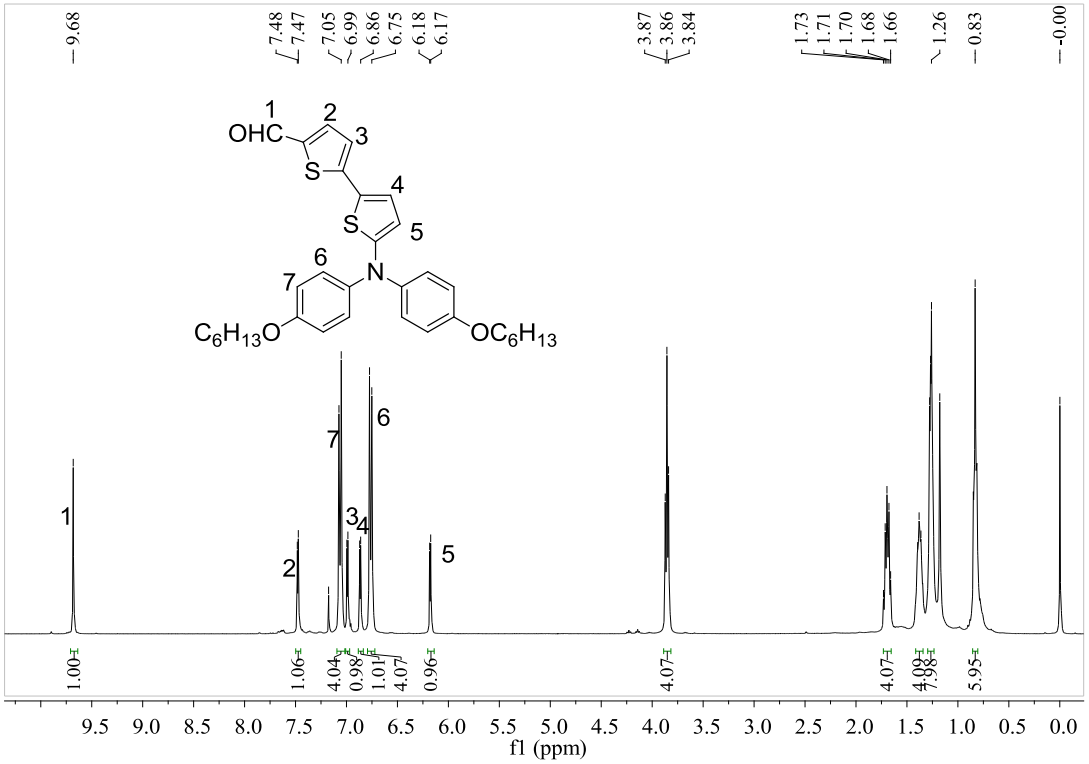

Compound **9**: ^{13}C NMR ($CDCl_3$, 100 MHz):

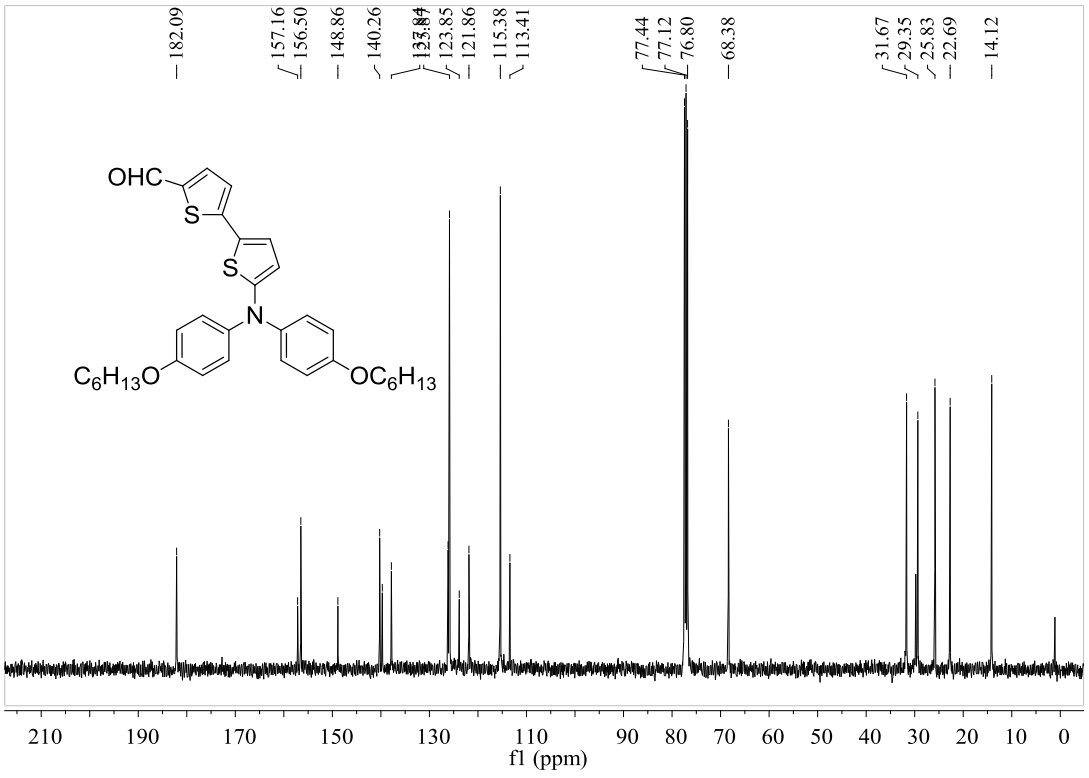

Compound **1**: ^{1}H NMR ($CDCl_3$, 400 MHz):

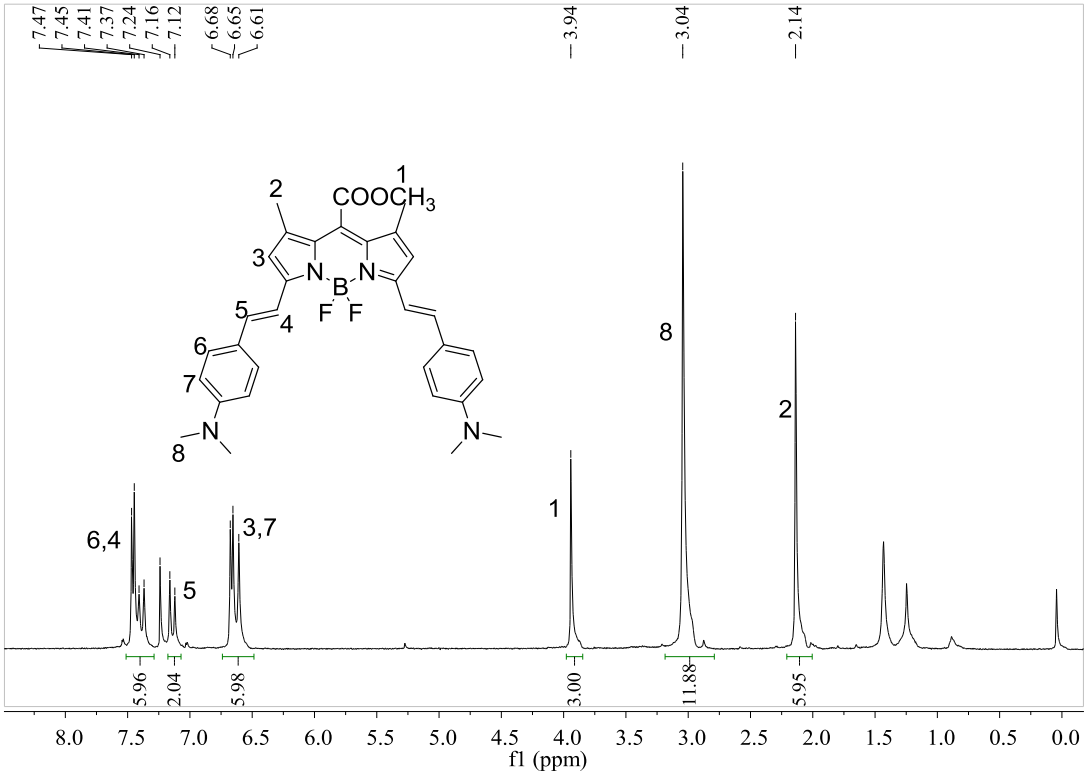

Compound **1**: ^{13}C NMR ($CDCl_3$, 100 MHz):

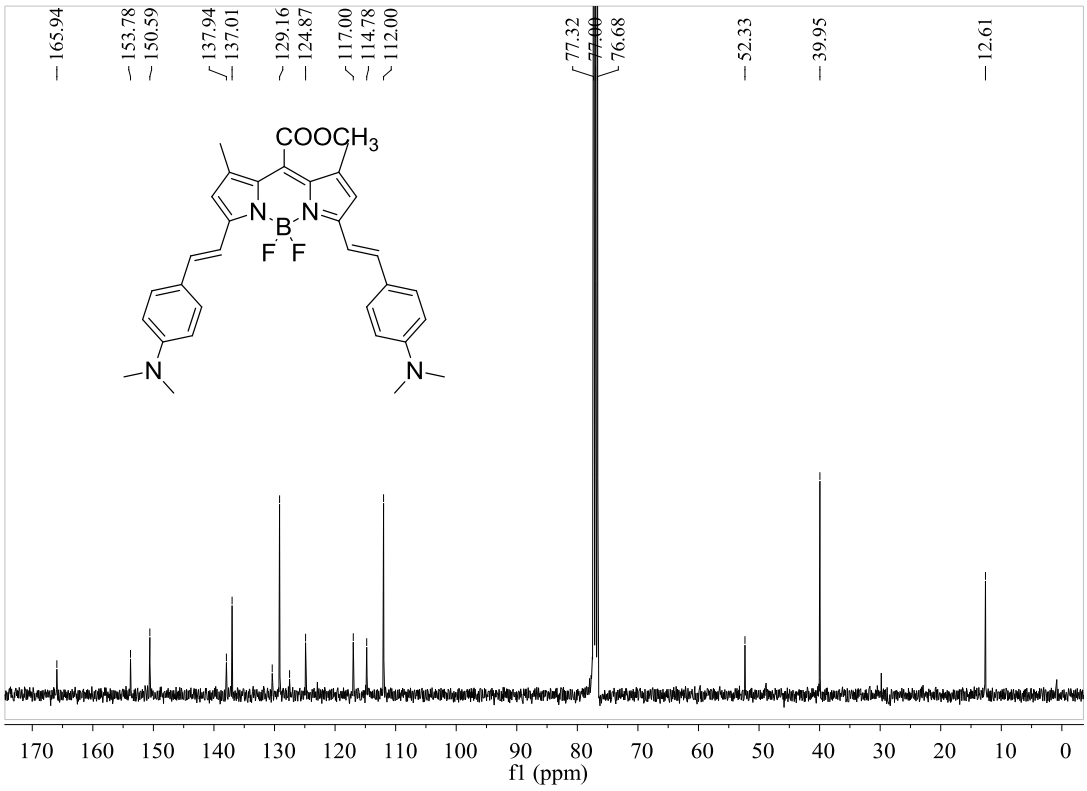

Compound **2**: ^{1}H NMR ($CDCl_3$, 400 MHz)

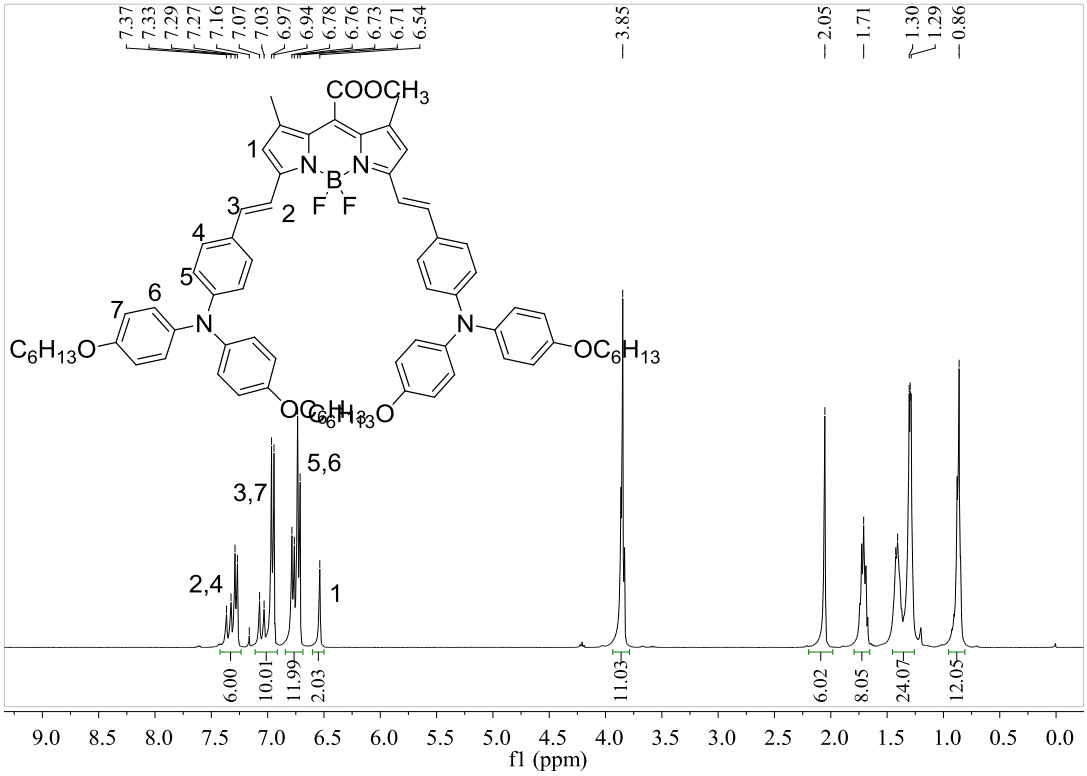

Compound **2**: ^{13}C NMR (d6-DMSO, 100 MHz)

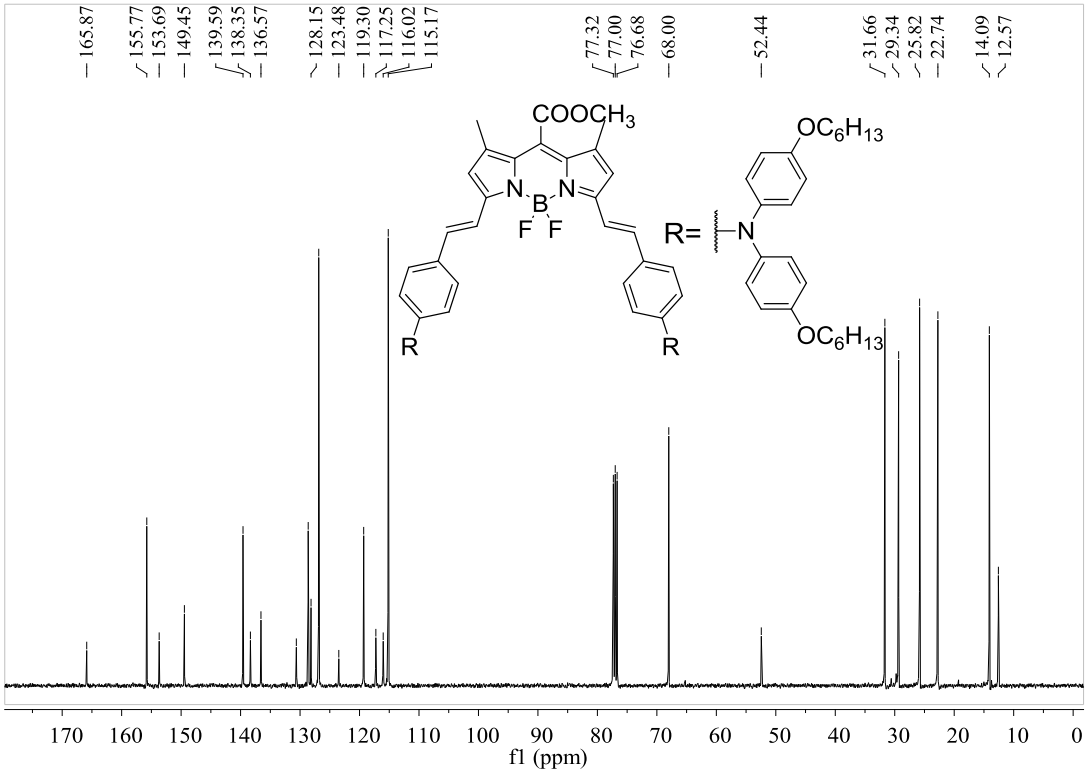

Compound **3**: ^{1}H NMR ($CDCl_3$, 400 MHz). The broadening is due to aggregation.

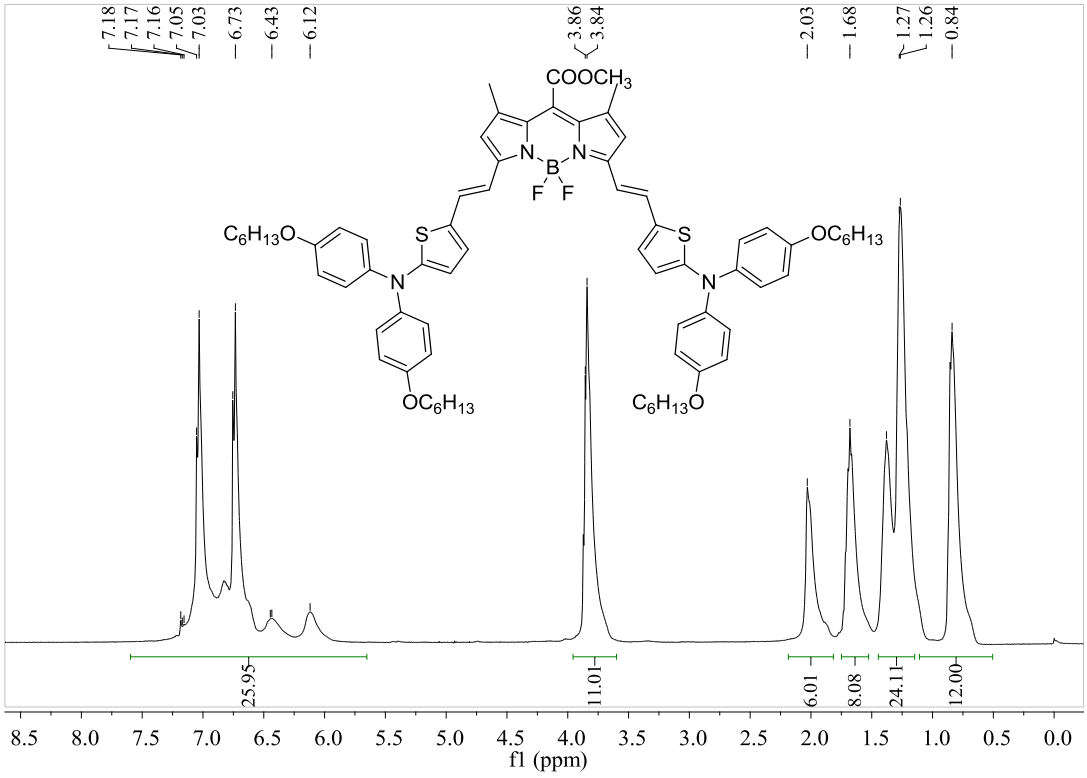

Compound **3**: ^{13}C NMR ($CDCl_3$, 100 MHz)

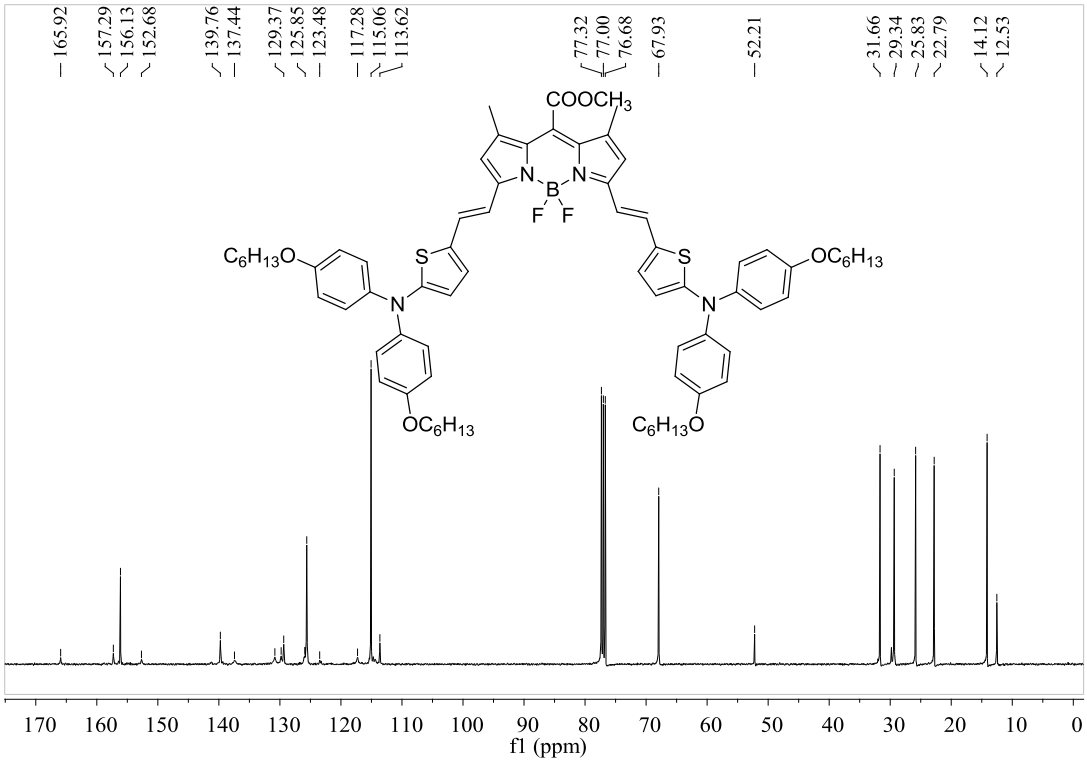

Compound **4**: ^{1}H NMR ($CDCl_3$, 400 MHz)

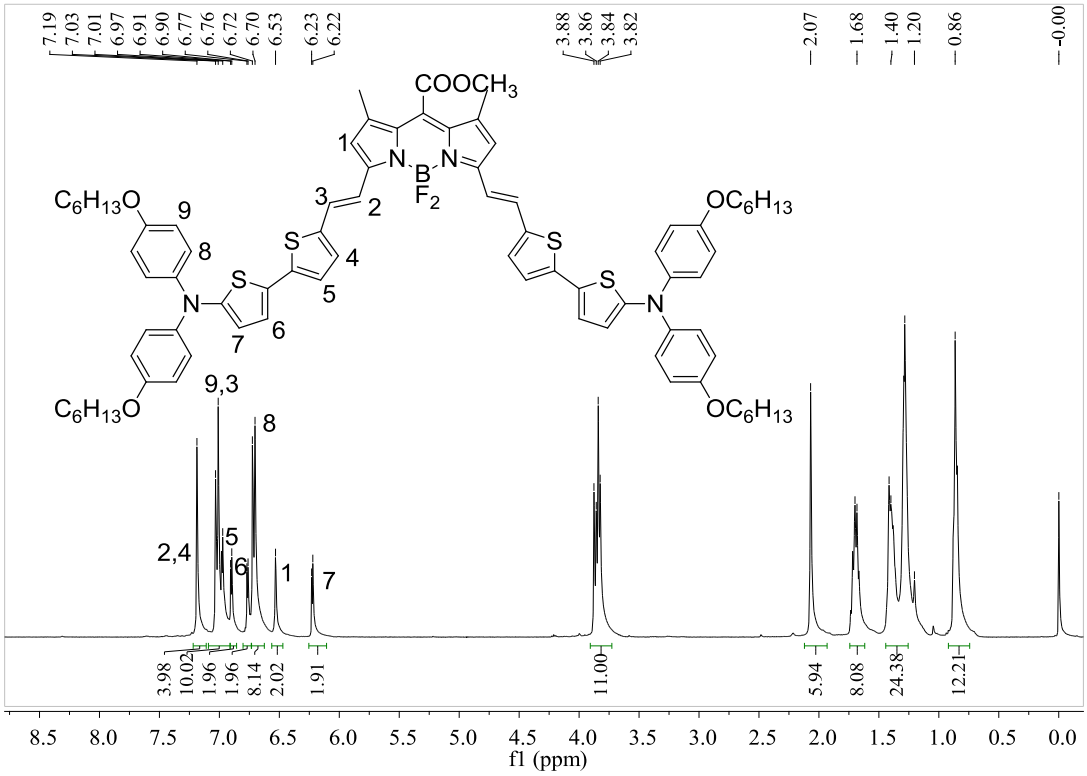

Compound **4**: ^{13}C NMR ($CDCl_3$, 100 MHz)

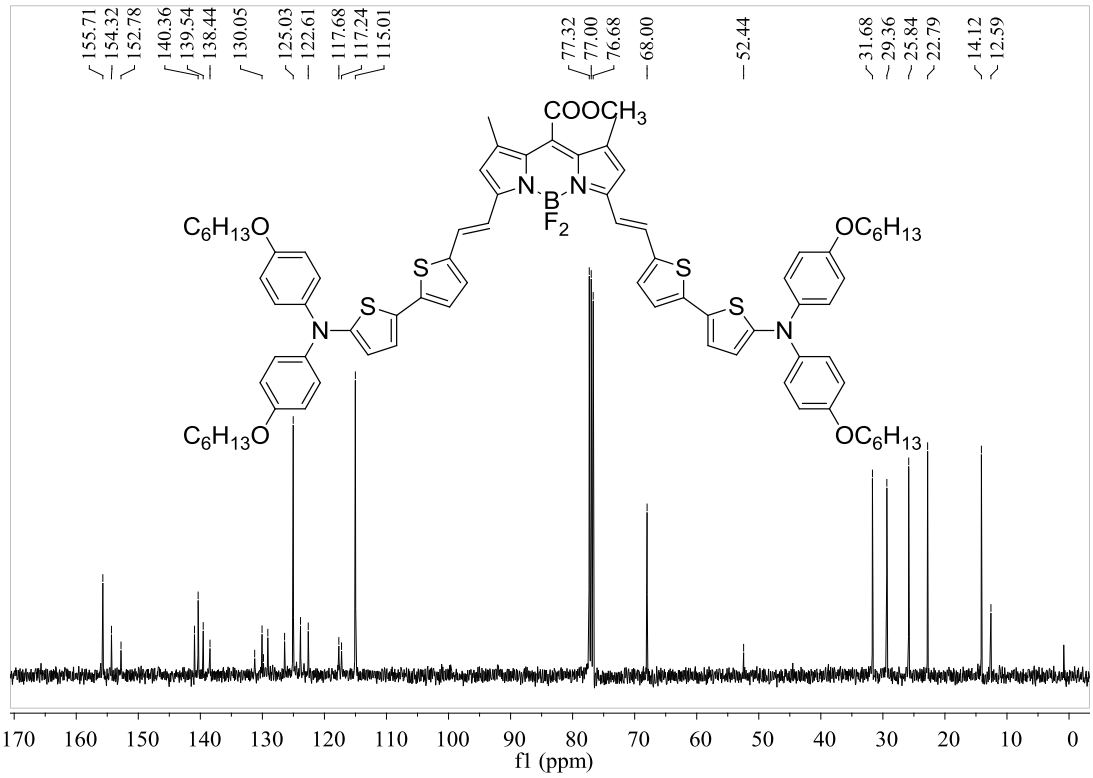

HR-ESI and HR-MALDI TOF mass spectra of all products

Compound **8**:

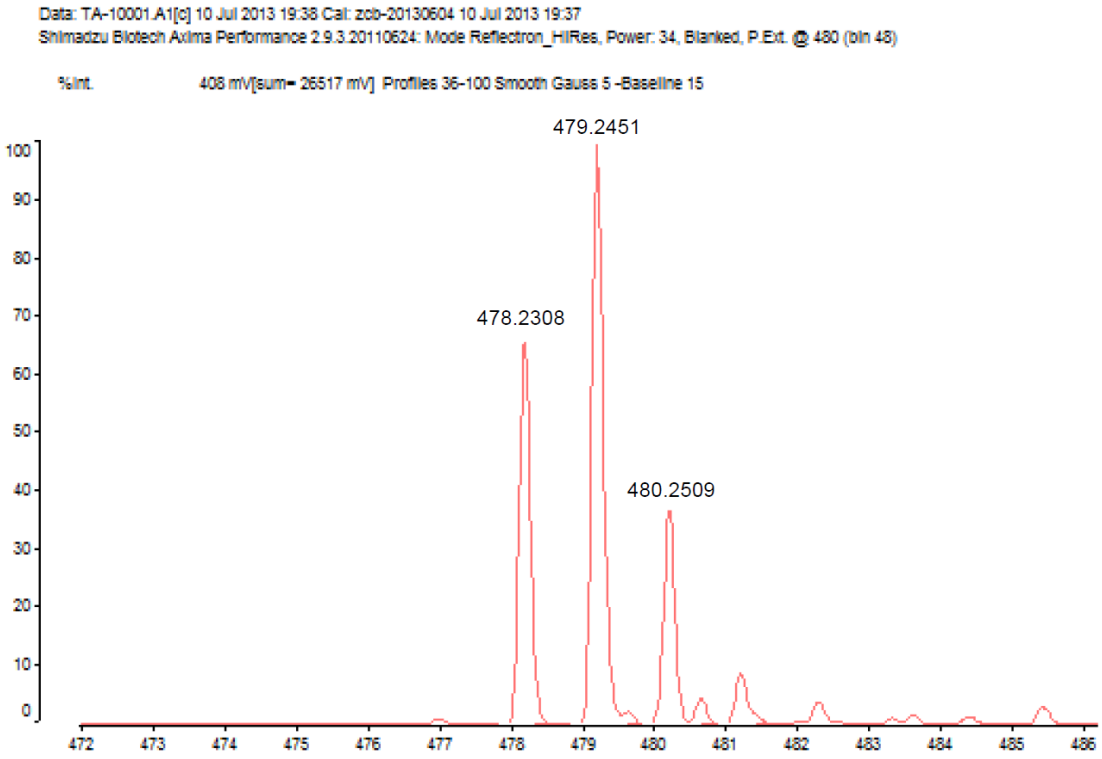

Compound **9**:

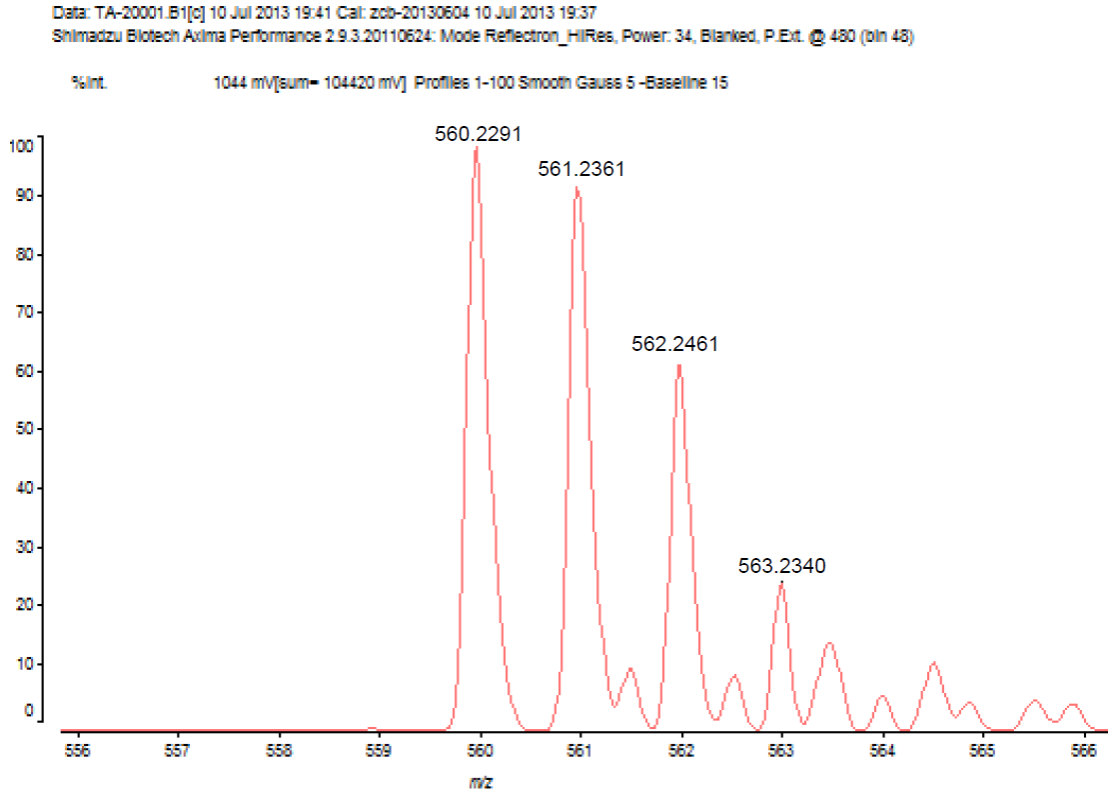

Compound **1**:

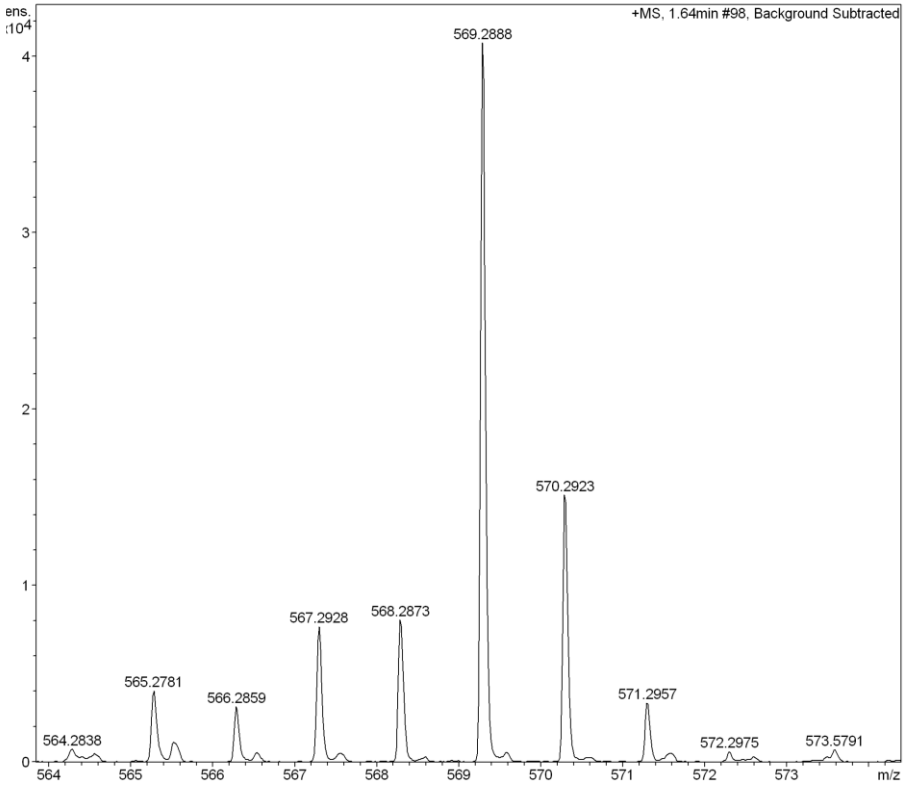

Compound **2**:

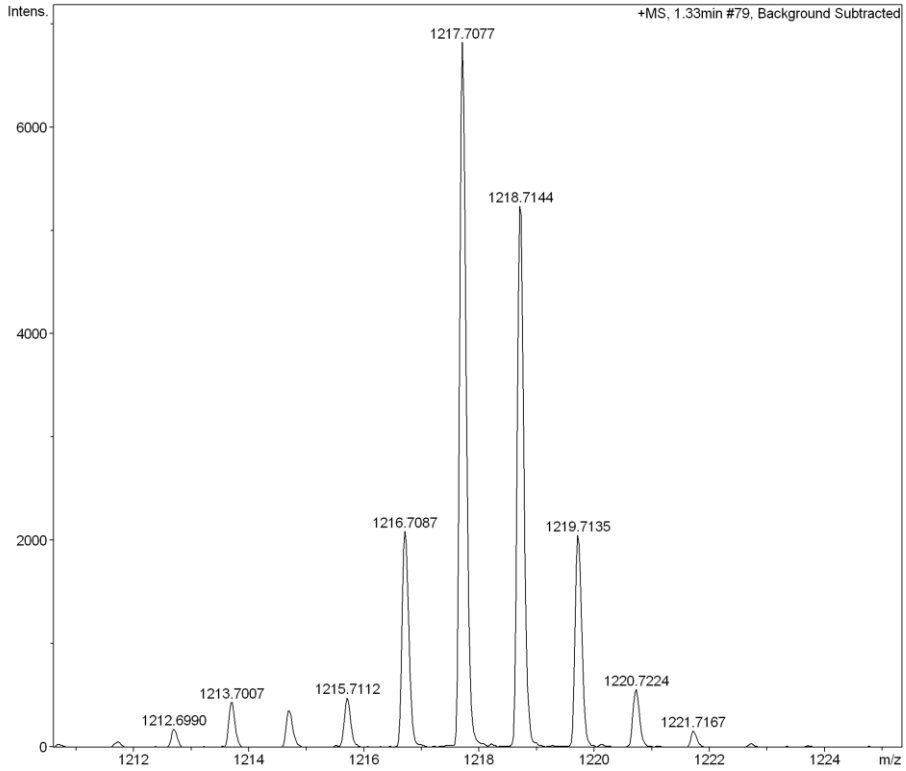

Compound **3**:

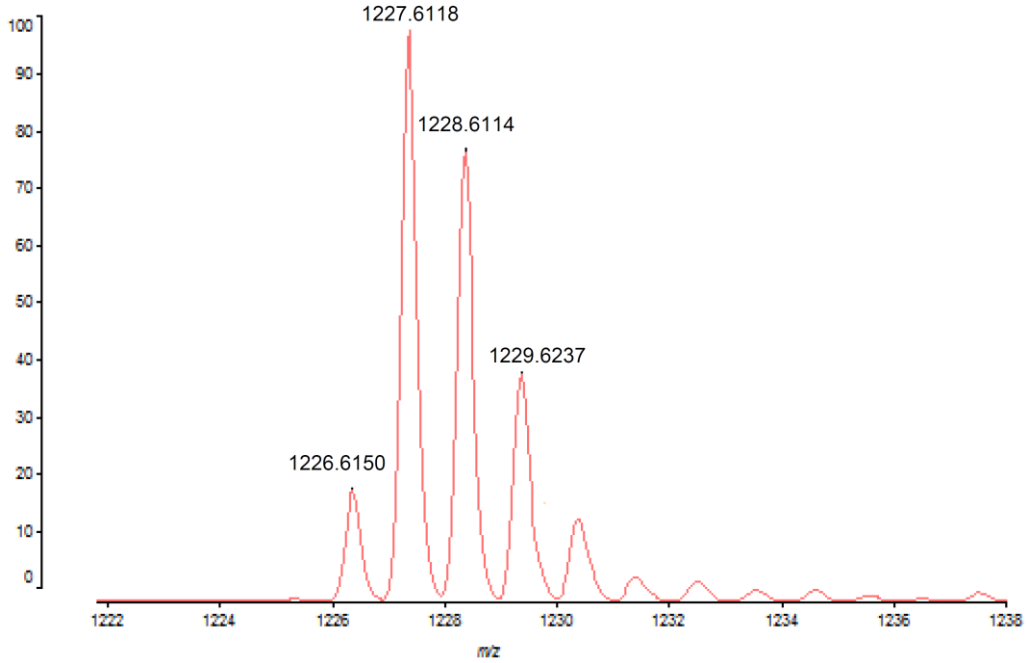
1227.6118
1228.6114
1229.6237
1226.6150
100
90
80
70
60
50
40
30
20
10
0
1222
1224
1226
1228
1230
1232
1234
1236
1238
m/z

Compound **4**:

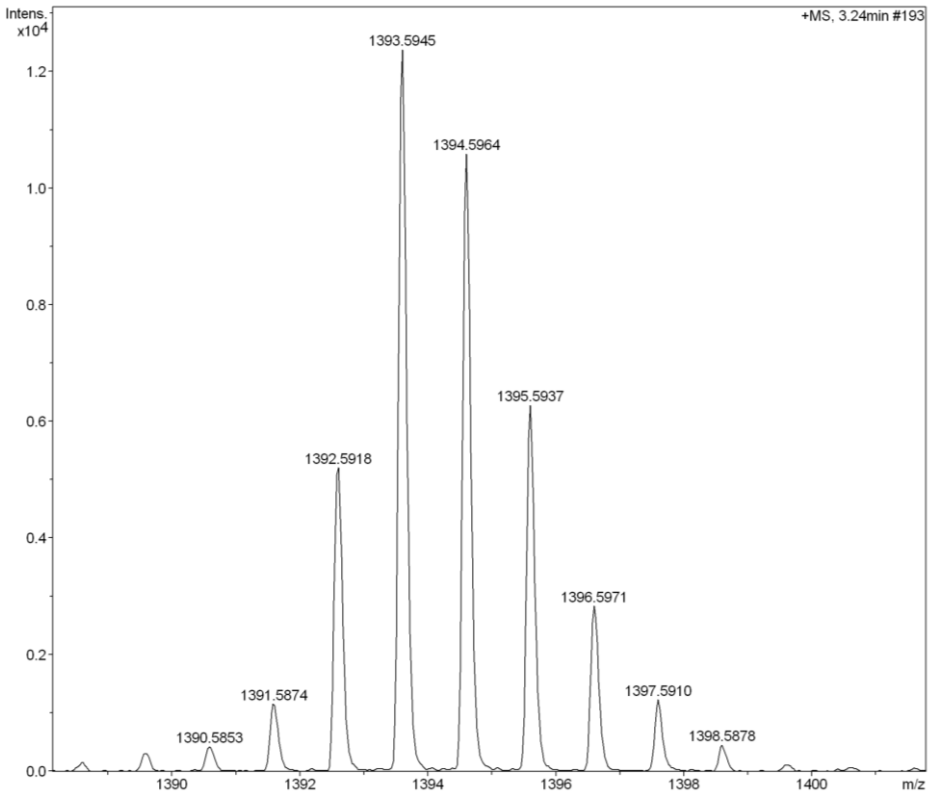
Intens.
x10^4
+MS, 3.24min #193
1393.5945
1394.5964
1395.5937
1392.5918
1396.5971
1391.5874
1397.5910
1390.5853
1398.5878
1.2
1.0
0.8
0.6
0.4
0.2
0.0
1390
1392
1394
1396
1398
1400
m/z

8. References

1. Ni, Y.; Zeng, L.; Kang, N.; Huang, K.; Wang, L.; Zeng, Z.; Chang, Y. -T.; Wu, J. *Chem. Eur. J.* **2014**, *20*, 2301.

2. (a) Becke, A. D. *J. Chem. Phys.* **1993**, *98*, 5648. (b) Lee, C.; Yang, W.; Parr, R. G. *Phys. Rev. B: Condens. Matter* **1988**, *37*, 785. (c) Yanai, T.; Tew, D.; and Handy, N. *Chem. Phys. Lett.* **2004**, *393*, 51. (d) Ditchfield, R.; Hehre, W. J.; Pople, J. A. *J. Chem. Phys.* **1971**, *54*, 724. (e) Hehre, W. J.; Ditchfield R.; Pople, J. A. *J. Chem. Phys.* **1972**, *56*, 2257. (f) Hariharan, P. C.; Pople, J. A. *Theor. Chim. Acta* **1973**, *28*, 213.

3. *Gaussian 09; Revision A.2*; Frisch, M. J.; Trucks, G. W.; Schlegel, H. B.; Scuseria, G. E.; Robb, M. A.; Cheeseman, J. R.; Scalmani, G.; Barone, V.; Mennucci, B.; Petersson, G. A.; Nakatsuji, H.; Caricato, M.; Li, X.; Hratchian, H. P.; Izmaylov, A. F.; Bloino, J.; Zheng, G.; Sonnenberg, J. L.; Hada, M.; Ehara, M.; Toyota, K.; Fukuda, R.; Hasegawa, J.; Ishida, M.; Nakajima, T.; Honda, Y.; Kitao, O.; Nakai, H.; Vreven, T.; Montgomery, J., J. A.; Peralta, J. E.; Ogliaro, F.; Bearpark, M.; Heyd, J. J.; Brothers, E.; Kudin, K. N.; Staroverov, V. N.; Kobayashi, R.; Normand, J.; Raghavachari, K.; Rendell, A.; Burant, J. C.; Iyengar, S. S.; Tomasi, J.; Cossi, M.; Rega, N.; Millam, N. J.; Klene, M.; Knox, J. E.; Cross, J. B.; Bakken, V.; Adamo, C.; Jaramillo, J.; Gomperts, R.; Stratmann, R. E.; Yazyev, O.; Austin, A. J.; Cammi, R.; Pomelli, C.; Ochterski, J. W.; Martin, R. L.; Morokuma, K.; Zakrzewski, V. G.; Voth, G. A.; Salvador, P.; Dannenberg, J. J.; Dapprich, S.; Daniels, A. D.; Farkas, Ö.; Foresman, J. B.; Ortiz, J. V.; Cioslowski, J.; Fox, D. J.; Gaussian, Inc., Wallingford CT, **2009**.